nature astronomy

LETTERS

PUBLISHED: 13 MARCH 2017 | VOLUME: 1 | ARTICLE NUMBER: 0063

Thermally anomalous features in the subsurface of Enceladus's south polar terrain

A. Le Gall[1]*, C. Leyrat[2], M. A. Janssen[3], G. Choblet[4], G. Tobie[4], O. Bourgeois[4], A. Lucas[5,6], C. Sotin[3,4], C. Howett[7], R. Kirk[8], R. D. Lorenz[9], R. D. West[3], A. Stolzenbach[1], M. Massé[4], A. H. Hayes[10], L. Bonnefoy[11], G. Veyssière[12] and F. Paganelli[13]

Saturn's moon Enceladus is an active world. In 2005, the Cassini spacecraft witnessed for the first time water-rich jets venting from four anomalously warm fractures (called sulci) near its south pole[1,2]. Since then, several observations have provided evidence that the source of the material ejected from Enceladus is a large underground ocean, the depth of which is still debated[3–6]. Here, we report on the first and only opportunity that Cassini's RADAR instrument[7,8] had to observe Enceladus's south polar terrain closely, targeting an area a few tens of kilometres north of the active sulci. Detailed analysis of the microwave radiometry observations highlights the ongoing activity of the moon. The instrument recorded the microwave thermal emission, revealing a warm subsurface region with prominent thermal anomalies that had not been identified before. These anomalies coincide with large fractures, similar or structurally related to the sulci. The observations imply the presence of a broadly distributed heat production and transport system below the south polar terrain with 'plate-like' features and suggest that a liquid reservoir could exist at a depth of only a few kilometres under the ice shell at the south pole. The detection of a possible dormant sulcus further suggests episodic geological activity.

The Cassini spacecraft (NASA (National Aeronautics and Space Administration), the European Space Agency and the Italian Space Agency) has explored the Saturnian system for the past 12 years. The detection of water-rich jets erupting from four large fractures (also called sulci, or informally, the 'tiger stripes') near the south pole of Enceladus is one of the major discoveries of the mission[1,2]. These jets are evidence for ongoing internal activity at Enceladus, whose south polar terrain (SPT) is anomalously warm and radiates an endogenic power of up to ~16 GW as indicated by thermal infrared data[9,10]. The detection of sodium salts[3] in the icy grains ejected from Enceladus, together with topography and gravity data[4,5], strongly suggest that the moon hides a reservoir of liquid water beneath its surface. The recent detection of a large physical libration[6] provides the first evidence for a global ocean underneath a relatively thin ice shell, potentially as thin as 5–10 km in the SPT. This ocean may harbour hydrothermal activity on its floor[11] and Enceladus is therefore one of the most promising environments suitable for extant life in the Solar System.

On 6 November 2011, during the closest approach of the 16th Enceladus encounter (flyby E16), the RADAR system[7,8] onboard the Cassini spacecraft had an opportunity to observe closely Enceladus's SPT. At a distance of ~500 km from the surface, the instrument acquired a synthetic aperture radar (SAR) image (Fig. 1a) and recorded the 2.2-cm-wavelength thermal emission (Fig. 1b) of an arc-shaped region, which is ~500 km long and ~25 km wide, centred at 63° S and 295° W, and located 30–50 km north of the thermally active sulci identified as the sources of Enceladus's jets. The calibrated surface brightness temperatures measured during E16 cover a range from $32.0^{+0.6}_{-2.6}$ to $60.0^{+1.2}_{-4.8}$ K. Herein, we demonstrate that these temperatures, like those measured over the SPT in the infrared[9,10], are too high for a purely exogenic explanation, with implications for endogenic processes and heat transport in Enceladus's SPT.

Microwave radiometers can be used to detect subsurface activity occurring at temperatures much lower and at depths much greater than those sampled by infrared instruments[12–14]. The Cassini radiometer measures a surface brightness temperature (T_b) that, as per the Rayleigh-Jeans law applicable at the 2.2 cm wavelength, is the product of the surface emissivity (e) and the effective physical temperature (T_{eff}), or the vertical temperature profile weighted by a radiative transfer function and integrated over depth: $T_b = eT_{eff}$. The mean emission depth, or penetration depth, into icy regoliths is typically 10 to 100 wavelengths (ref. [15]), which translates into several tens of centimetres up to a few metres for the Cassini radiometer.

Interestingly, the region observed by the Cassini RADAR during the closest approach of E16 was entirely in cold darkness: one part was on the night side of Enceladus while the other was experiencing a solar eclipse. However, where the penetration depth is large enough, the temperatures sensed by the Cassini radiometer are dominated by the seasonal signal and thus decoupled from the surface conditions (for example, ref. [16]). This is key for the analysis of the E16 radiometry observations, which occurred shortly after the vernal Equinox; that is, at a time when a significant amount of

[1]LATMOS/IPSL, UVSQ Université Paris-Saclay, UPMC Université de Paris 06, CNRS, 78280 Guyancourt, France. [2]LESIA, Observatoire de Paris, PSL-Research University, CNRS, Université Pierre et Marie Curie Paris 06, Université Paris-Diderot, 92195 Meudon France. [3]Jet Propulsion Laboratory, California Institute of Technology, Pasadena, California 91109, USA. [4]Laboratoire de Planétologie et Géodynamique de Nantes, Université Nantes Atlantique, 44322 Nantes Cedex 3, France. [5]Laboratoire Astrophysique, Instrumentation et Modélisation, CNRS-UMR 7158, Université Paris-Diderot, CEA-Saclay, 91191 Gif sur Yvette, France. [6]Institut Physique du Globe de Paris, Université Paris-Diderot, USPC, 75205 Paris Cedex 13 France. [7]Southwest Research Institute, Boulder, Colorado 80302, USA. [8]US Geological Survey, Flagstaff, Arizona 86001, USA. [9]Johns Hopkins Applied Physics Laboratory, Laurel, Maryland 20723, USA. [10]Center for Radiophysics and Space Research, Cornell University, Ithaca, New York 14853, USA. [11]Lunar and Planetary Laboratory, University of Arizona, Tucson, Arizona 85721, USA. [12]CNRM-GAME, Météo-France, and CNRS, 31057 Toulouse Cedex 1 France. [13]American Public University System, Charles Town, West Virginia 25414, USA. *e-mail: alice.legall@latmos.ipsl.fr

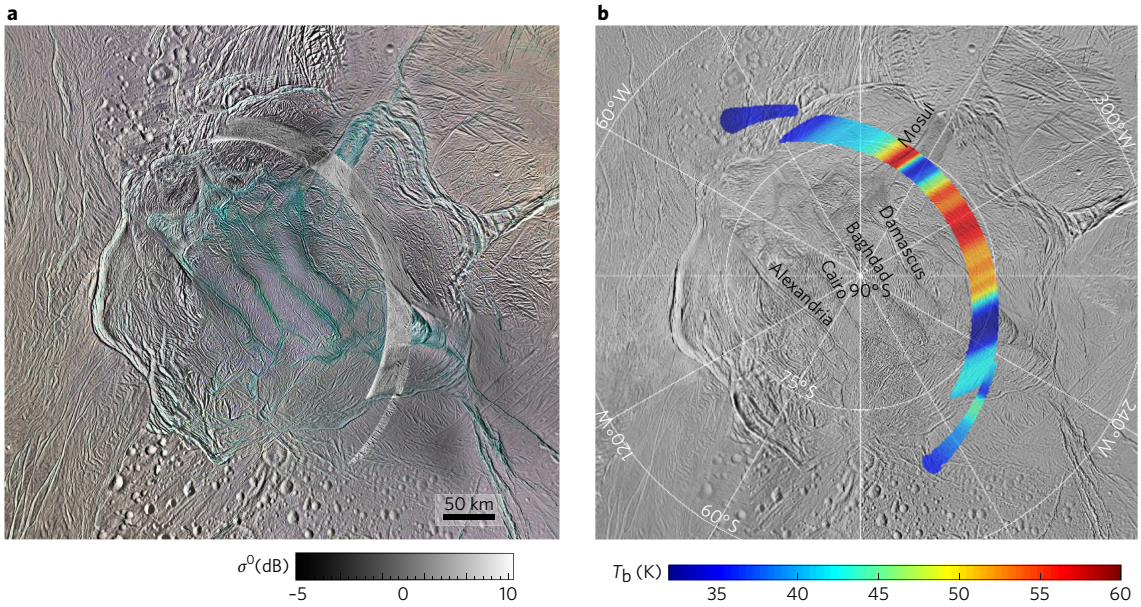

Figure 1 | Stereographic polar projection of active and passive RADAR observations of Enceladus's SPT acquired during the closest approach of flyby E16. a, E16 SAR image (resolution: ~50 m and ~200 m in the cross- and along-track directions, respectively) overlaying a colour mosaic produced by the Cassini ISS (PIA18435). The mapped region includes part of the Mosul Sulci system and two V-shaped regions (near the western and eastern ends of the swath) exhibiting especially high backscattering cross-sections σ^0. **b**, E16 surface brightness-temperature map (wavelength, 2.2 cm; resolution, ~4 km × 25 km in the middle of the swath) overlaying a visible-light ISS mosaic (PIA14937). Radiometer measurement footprints are long and narrow ellipses with the long axis roughly in the cross-track direction. The measured brightness temperatures cover a range from $32.0^{+0.6}_{-2.6}$ to $60.0^{+1.2}_{-4.8}$ K.

heat had been stored in the south polar regions from the previous summer. Thermal simulations show that the buried heat and the contribution from Saturn's infrared thermal emission (the main source of heating during a solar eclipse) can increase the effective temperature by up to 5 K, compared with the surface temperature, and predict a maximum $T_{\rm eff}$ of 60 K.

Only a fraction (e) of the thermal energy is emitted by radiation from Enceladus's surface and detected by the Cassini radiometer. Distant observations have shown that Enceladus has one of the lowest disk-averaged 2.2 cm emissivities in the Saturnian system, namely ~0.6–0.7 (ref. [17,18]). This is due to a volume scattering mechanism (for example, ref. [19]): the transparency and porosity of Enceladus's clean water ice regolith provides enhanced opportunity for scattering, which prevents the emitted waves from escaping the subsurface.

More specific constraints on Enceladus's surface 2.2 cm emissivity along the E16 track can be derived from concurrent active measurements (Fig. 1a), by virtue of Kirchhoff's law of radiation. Although we also considered the case of a Lambertian (that is, isotropically diffuse) surface (hereafter LS), we found that the combined emissivity–backscatter model proposed in ref. [20] for a surface presuming a volume scattering medium including the effects of polarization and coherent backscattering (CBE, which is the reflection enhancement around the backscatter direction that may occur with high-order scattering; see ref. [21] for example) best reproduces the E16 radiometry measurement variations, pointing to maximum emissivities in the range 0.40–0.85. Surfaces described by this model are hereafter referred to as diffuse scattering surfaces (DSS) with CBE.

With our thermal, radiative transfer and emissivity models, we estimated the maximum expected brightness temperatures in the absence of endogenic flux and compared them with the E16 radiometry observations. This revealed that the measured $T_{\rm b}$ values were too high to be caused by the simple thermal re-radiation of the light absorbed at the surface and require a buried heat source. Figure 2 displays the excess of flux once the maximum predicted passive thermal background has been subtracted from the radiometry measurements considering an LS (Fig. 2a) and a DSS with CBE (Fig. 2b). The thermal anomaly is especially pronounced over two or three areas.

First, thermal anomalies—with a peak value of $1.1^{+0.2}_{-0.5}$ W m^{-2} for an LS and $3.0^{+0.2}_{-1.0}$ W m^{-2} for a DSS with CBE—appear coincident with one or two curved scarps associated with sharp elevation changes (up to ~1 km (ref. [22])) and the bounding radar-bright V-shaped discontinuities located at the eastern and western ends of the swath (Fig. 2c,e). The broken-up appearance of these discontinuities in the SAR image and their blue colour in Cassini Imaging Science Subsystem (ISS) images suggest the presence of coarse-grained ice, like in the active sulci, and thus recent activity[23].

Second, a thermal anomaly appears in the centre of the E16 track where the most prominent surface landform is a 2 km-wide, tens-of-km-long and ~650 m-deep linear fracture (Fig. 2c,f), similar in appearance to the 'tiger stripes' and running roughly parallel to them. If a localized thermal anomaly is indeed associated with this fracture, it is at least three times larger in amplitude than indicated in Fig. 2a,b, where it is diluted in the wide instrument footprint that is perpendicular to the feature. The nearby smaller fractures may also contribute to the measured thermal signal.

No jet has been observed in the region of interest. Nor do 9–17-μm-wavelength observations by Cassini's Composite Infrared Spectrometer (CIRS) show any obvious hint of endogenic emission (Fig. 2d). However, this is readily explained by both the poor sensitivity to low temperatures (<65 K) at short wavelengths and the different penetration depths of infrared and radio waves. The linear fracture at the centre of the E16 swath could be a 'dormant' or 'dying' sulcus: too cold at the surface to be distinguished from the passive thermal background by CIRS and/or masked by a thermally insulating layer of frost (for example, one formed from plume particle fallout) but warm a few metres below.

In addition to warm individual features, the model for a DSS with CBE argues in favour of a broadly distributed heat source below Enceladus's SPT with a mean heat output (once the contribution from the three features mentioned above is removed) of

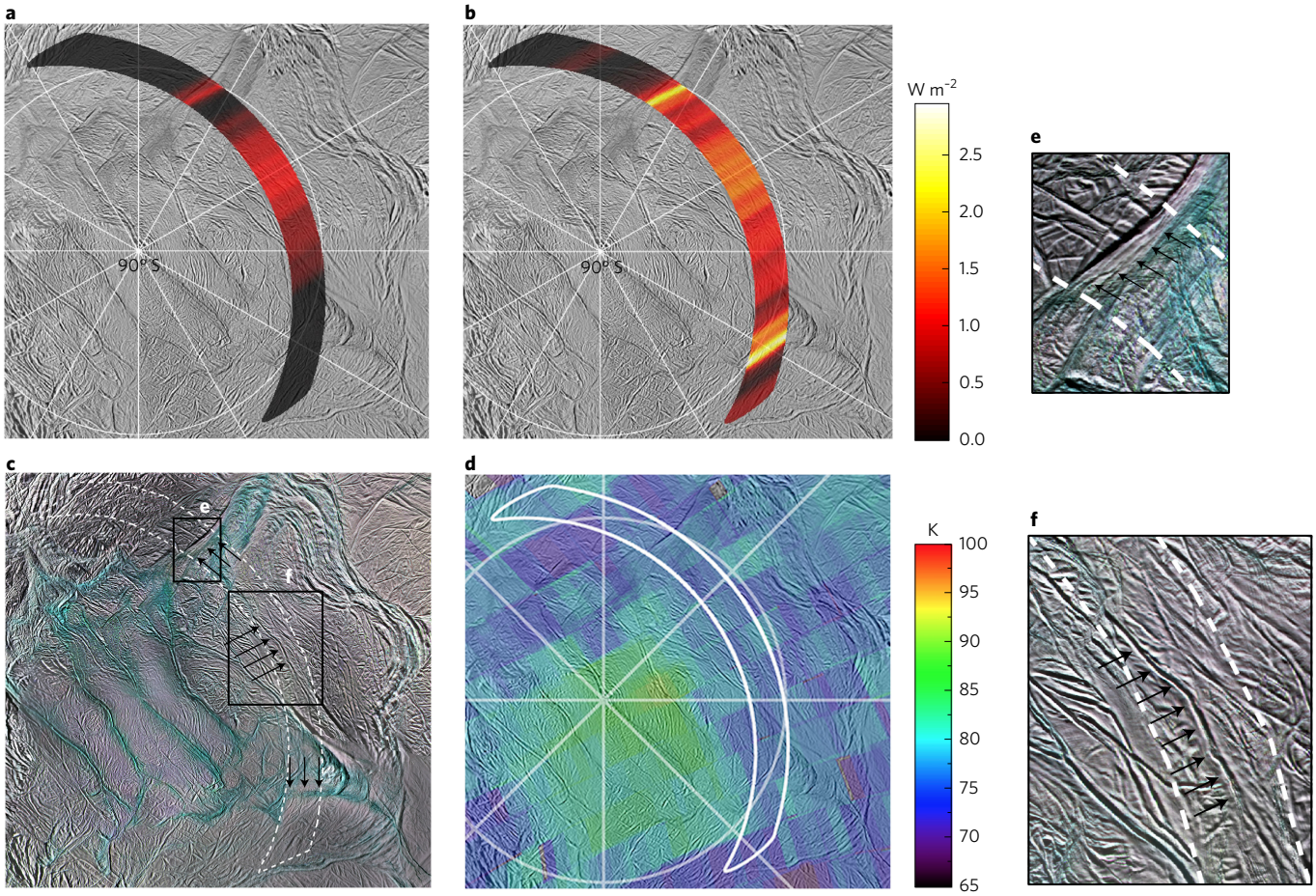

Figure 2 | Thermal anomalies along the E16 RADAR track. a,**b**, Minimum heat fluxes in excess as derived from the microwave radiometry observations assuming an LS (**a**) or a DSS with CBE (**b**). **c**, ISS colour mosaic of Enceladus's SPT with the three main surface features associated with peak heat outputs on **a** and **b** indicated by arrows. **d**, Map of CIRS observations of the SPT (wavelength, 9–17 μm; resolution, ~25–30 km per pixel) with the E16 swath outlined in white. **e**,**f**, Close-up ISS images of the curved scarp part of the Mosul Sulci system (**e**) and of the possible dormant sulcus located in the middle of the E16 track (**f**).

at least 0.5 W m^{-2}. This value agrees well with the average excess flux derived from CIRS 17–1,000-μm-wavelength measurements over Enceladus's SPT (~0.4–0.5 W m^{-2} (ref. [10])) and with the estimate of the heat flux arising (probably currently) from the deformed funiscular terrains between the sulci (potentially as high as 0.4 W m^{-2} (ref. [24])).

A mean excess flux of ~0.5 W m^{-2} implies a very strong heat source beneath the surface, most probably endogenic in nature, and is consistent with the presence of liquid water at depths as small as 2 km beneath the central part of the SPT (see Supplementary Information), as suggested by the recent interpretation of the libration, topography and gravity data[25]. This implies a pronounced thinning of the ice shell in the SPT (<5 km), and abrupt thickening in the surrounding terrains (cl_3 unit in Fig. 3a and ref. [26]).

The only known heating mechanism capable of generating sustained temperature increases like those observed is tidal dissipation driven by the rhythmic distortions of Enceladus as it follows its eccentric orbit around Saturn[1]. Unlike for large moons such as Europa or Titan (for example, ref. [27]), tidal deformation within Enceladus's ice shell is very sensitive to its thickness (for example, ref. [28]): shell thinning results in a strong increase in tidal deformation and hence in the production of heat by both viscous dissipation and shear heating along faults[25].

The four 'tiger stripes' of Enceladus are most probably located in the thinnest part of the SPT. In contrast, according to ref. [25], the potential 'dying' or dormant sulcus (Fig. 2f) is in an area where the shell thickness is two to three times greater; that is, where tidal deformation and the connectivity with the subsurface ocean are reduced (Fig. 3b). This could explain why this fault is not currently a source of jets. It may have experienced eruption activity in the recent past when the ice shell was thinner and ceased its activity due to, for example, the subsurface ocean crystallization. Alternatively, it may be in a temporary or permanent dormant state if it takes more time or is simply impossible to trigger water eruptions in a thicker ice shell.

On the basis of their location at the boundary between the csp and cl_3 units (Fig. 3a), the warm scarps on the edge of the E16 swath (Fig. 2e) could be extensional faults related to the gravitational relaxation of the ice shell, as observed on Earth at the boundaries of regions of crustal thickness difference (for example, the Basin and Range[29]). Alternatively, they could indicate compression resulting from equatorward motion of material in response to crustal spreading at the 'tiger stripes'[30]; for example, analogous to seafloor spreading at terrestrial mid-ocean ridges. Enhancement of tidal heating in the SPT margins due to the complex tidal response of SPT faults[31] may also play a role, further increasing the thermal anomaly. In all cases, the activity would lead to the local upward deflection of the isotherms in the crust, thereby producing a strong local increase in the radial thermal gradient (Fig. 3b) and, hence, a heat flow anomaly.

We note that no sign of current endogenic activity has been indicated by the Cassini radiometer at Enceladus's lower latitudes. However, geological evidence (for example, ref. [26]) and estimates of

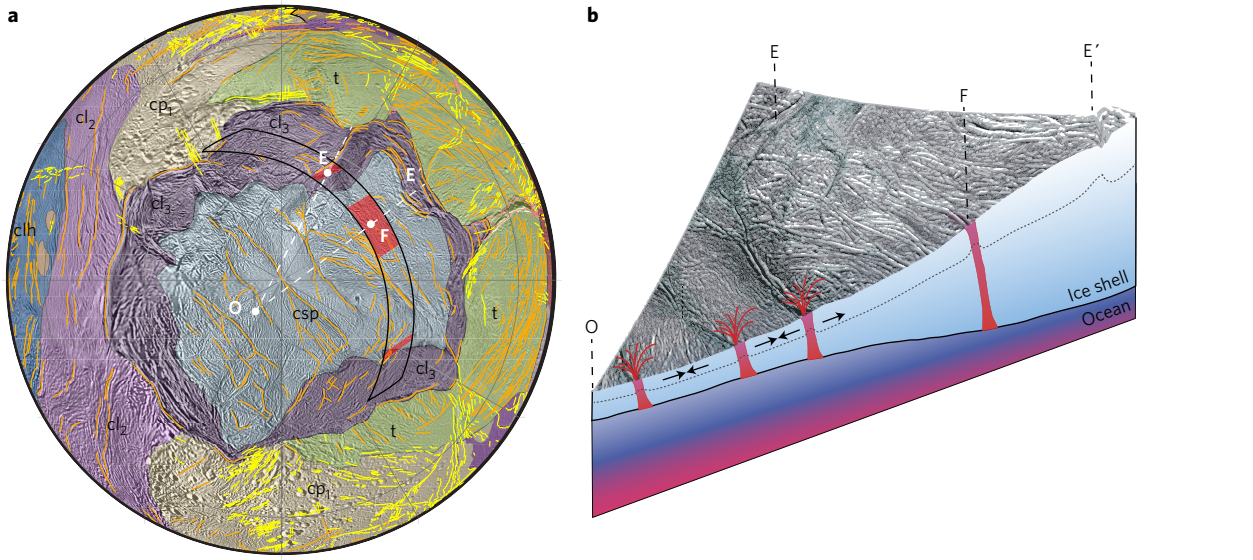

Figure 3 | Possible scenario for the heat production and transport in the subsurface of Enceladus's SPT. a, Orthographic projection of the SPT with the structural units mapped in ref. [26] superimposed. The E16 RADAR swath is outlined in black and the regions with a peak thermal anomaly are marked red. **b**, Notional sketch of the subsurface below the profiles, OE and OF (see **a**). Point E corresponds to one of the two identified warm curved scarps (probably similar to that in point E′) associated with an upward deflection of the isotherm. Point F corresponds to the possible dormant sulcus detected in the middle of the E16 track, in a region where the thickness of the ice shell is probably less than that below point E (or E′) but greater than that in the central SPT. The dotted line represents a subsurface isotherm and the arrows indicate the extensional and compressional stresses around the 'tiger stripes'.

palaeo-heat flows comparable to the SPT's present-day output (for example, ref. [32]) suggest that the leading and trailing sides have also experienced episodes of being in a dissipative state. The present detection of a possible dormant sulcus and of warm fractures at the edge of 'plate-like' features is a further argument for a non-steady state of Enceladus, involving a dynamical evolution of the ice shell. Subsurface radar sounding together with detailed surface mapping by a future exploration mission may reveal the complex subsurface dynamics of this active ocean world.

Methods

For the analysis of the Cassini radiometry data collected during the closest approach of flyby E16 (E16 passive radar data), we developed a model to predict the microwave thermal emission from Enceladus's surface in the absence of an endogenic heat source. In this approach we combined three models: (1) a thermal model providing the physical temperature–depth profile below the surface at the epoch of the E16 measurements and as a function of the thermal properties, (2) a radiative transfer model to infer the effective temperature (T_{eff}) sensed by the Cassini radiometer down to a given depth (namely the emission depth), and (3) an emissivity model (e) that relies on the combined emissivity–backscatter model proposed in ref. [20] and uses the concurrent E16 active radar data. These models are further described in the Supplementary Information. The thermal model, in particular, considers both diurnal and seasonal timescales of insolation and thermal variations, and takes into account solar eclipses that were daily at the time of the E16 flyby, as well as heating from Saturn (both from its infrared thermal and the sunlight reflected by its upper atmosphere). It was validated by comparison with Cassini's CIRS observations and other thermal models. Combined with a radiative transfer model, it was able to reproduce Cassini radiometry measurements at Iapetus and to predict Pluto's subsurface temperatures[16]. For the emissivity model, we explored two types of surface: an LS and a DSS with CBE. The DSS with CBE best reproduced the variations of the measured brightness temperatures along the E16 RADAR track. It is also the best suited class of surfaces for Titan's radar-brightest terrains which are potential analogues for Enceladus's terrains.

The free parameters of the global model were then adjusted to predict the maximum expected brightness temperatures ($T_{\mathrm{b}} = eT_{\mathrm{eff}}$ in the Rayleigh-Jeans domain) along the E16 RADAR track in the absence of an endogenic heat source. These predicted temperatures were compared with the measured ones, showing that the E16 radiometry measurements cannot be explained without invoking a buried heat source. The difference between predictions and measurements was used to estimate the minimum excess heat flux along the E16 track and the depth of a potential liquid layer assuming a pure-water ice shell (see Supplementary Information). One of the thermal anomalies seems to coincide with a large sulcus-like feature whose depth was estimated by radarclinometry (see Supplementary Information).

Data availability. The data reported in this paper are archived in the Planetary Data System: http://pdsimage.wr.usgs.gov/archive/co-v_e_j_s-radar-3-sbdr-v1.0/CORADR_0232/. The simulation results are available from A.L.G. on request.

Received 2 November 2016; accepted 24 January 2017; published 13 March 2017

References

1. Porco, C. C. *et al.* Cassini observes the active south pole of Enceladus. *Science* **311,** 1393–1401 (2006).
2. Spitale, J. N. & Porco, C. C. Association of the jets of Enceladus with the warmest regions on its south polar fractures. *Nature* **449,** 695–697 (2007).
3. Postberg, F. *et al.* Sodium salts in E-ring ice grains from an ocean below the surface of Enceladus. *Nature* **459,** 1098–1101 (2009).
4. Collins, G. C. & Goodman, J. C. Enceladus' south polar sea. *Icarus* **189,** 72–82 (2007).
5. Iess, L. *et al.* The gravity field and interior structure of Enceladus. *Science* **344,** 78–80 (2014).
6. Thomas, P. C. *et al.* Enceladus's measured physical libration requires a global subsurface ocean. *Icarus* **264,** 37–47 (2016).
7. Elachi, C. *et al.* RADAR: the Cassini Titan radar mapper. *Space Sci. Rev.* **115,** 71–110 (2004).
8. Janssen, M. A. *et al.* Titan's surface at 2.2-cm wavelength imaged by the Cassini RADAR radiometer: calibration and first results. *Icarus* **200,** 222–239 (2009).
9. Spencer, J. R. *et al.* Cassini encounters Enceladus: background and the discovery of a south polar hot spot. *Science* **311,** 1401–1405 (2006).
10. Howett, C. J. A., Spencer, J. R., Pearl, J. & Segura, & M. High heat flow from Enceladus' south polar region measured using 10–600 cm^{-1} Cassini/CIRS data. *J. Geophys. Res.* **116,** E03003 (2011).
11. Hsu, H.-W. *et al.* Ongoing hydrothermal activities within Enceladus. *Nature* **519,** 207–210 (2015).
12. Keihm, S. J. Interpretation of the lunar microwave brightness temperature spectrum: feasibility of orbital heat flow mapping. *Icarus* **60,** 568–589 (1984).
13. Bondarenko, N. V., Head, J. W. & Ivanov, M. A. Present-day volcanism on Venus: evidence from microwave radiometry. *Geophys. Res. Lett.* **37,** L23202 (2010).
14. Lorenz, R. D., Le Gall, A. & Janssen, M. A. Detecting volcanism on Titan and Venus with microwave radiometry. *Icarus* **270,** 30–36 (2016).
15. Paillou, P. *et al.* Microwave dielectric constant of Titan-relevant materials. *Geophys. Res. Lett.* **35,** L18202 (2008).

16. Leyrat, C., Lorenz, R. D. & Le Gall, A. Probing Pluto's underworld: ice temperatures from microwave radiometry decoupled from surface conditions. *Icarus* **268,** 50–55 (2016).
17. Ostro, S. J. *et al.* Cassini RADAR observations of Enceladus, Tethys, Dione, Rhea, Iapetus, Hyperion, and Phoebe. *Icarus* **183,** 479–490 (2006).
18. Ries, P. A. & Janssen, M. A. A large-scale anomaly in Enceladus' microwave emission. *Icarus* **257,** 88–102 (2015).
19. Black, G. J., Campbell, D. B. & Nicholson, P. D. Icy Galilean satellites: modeling radar reflectivities as a coherent backscattering effect. *Icarus* **151,** 167–180 (2001).
20. Janssen, M. A., Le Gall, A. & Wye, L. C. Anomalous radar backscatter from Titan's surface? *Icarus* **212,** 321–328 (2011).
21. Hapke, B. Coherent backscatter and the radar characteristics of outer planet satellites. *Icarus* **88,** 407–417 (1990).
22. Nahm, A. L. & Kattenhorn, S. A. A unified nomenclature for tectonic structures on the surface of Enceladus. *Icarus* **258,** 67–81 (2015).
23. Schenk, P. M. *et al.* Plasma, plumes and rings: Saturn system dynamics as recorded in global color patterns on its midsize icy satellites. *Icarus* **211,** 740–757 (2011).
24. Bland, M. T., McKinnon, W. B. & Schenk, P. M. Constraining the heat flux between Enceladus' tiger stripes: numerical modeling of funiscular plains formation. *Icarus* **260,** 232–245 (2015).
25. Čadek, O. *et al.* Enceladus's internal ocean and ice shell constrained from Cassini gravity, shape, and libration data. *Geophys. Res. Lett.* **43,** 5653–5660 (2016).
26. Crow-Willard, E. N. & Pappalardo, R. T. Structural mapping of Enceladus and implications for formation of tectonized regions. *J. Geophys. Res. Planets* **120,** 928–950 (2015).
27. Tobie, G., Mocquet, A. & Sotin, C. Tidal dissipation within large icy satellites: applications to Europa and Titan. *Icarus* **177,** 534–549 (2005).
28. Nimmo, F., Spencer, J. R., Pappalardo, R. T. & Mullen, M. E. Shear heating as the origin of the plumes and heat flux on Enceladus. *Nature* **447,** 289–291 (2007).
29. Rey, P., Vanderhaeghe, O. & Teyssier, C. Gravitational collapse of the continental crust: definition, regimes and modes. *Tectonophysics* **342,** 435–449 (2001).
30. Gioia, G., Chakrobarty, P., Marshak, S. & Kieffer, S. W. Unified model of tectonics and heat transport in a frigid Enceladus. *Proc. Natl Acad. Sci. USA* **104,** 13578–13581 (2007).
31. Souček, O., Hron, J., Běhounková, M. & Čadek, O. Effect of the tiger stripes on the deformation of Saturn's moon Enceladus. *Geophys. Res. Lett.* **43,** 7417–7423 (2016).
32. Bland, M. T., Singer, K. N., McKinnon, W. B. & Schenk, P. M. Enceladus' extreme heat flux as revealed by its relaxed craters. *Geophys. Res. Lett.* **39,** L17204 (2012).

Acknowledgements

The authors wish to thank the Cassini-Huygens team for the design, development and operation of the mission. The Cassini-Huygens mission is a joint endeavour of NASA, the European Space Agency (ESA) and the Italian Space Agency (ASI), and it is managed by the Jet Propulsion Laboratory, California Institute of Technology under a contract with NASA. Most of the authors of this work are members or associate members of the Cassini RADAR Team. A.L.G. gratefully acknowledges the support of the French Space Agency, CNES, and the Université de Versailles Saint-Quentin (UVSQ) (Chair CNES/UVSQ). R.L. acknowledges the support of the NASA grant, NNX13AH14G 'Cassini RADAR Science Support'. A.L. acknowledges the financial support of the UnivEarthS Labex programme at Sorbonne Paris Cité (ANR-10-LABX-0023 and ANR-11-IDEX-0005-02).

Author contributions

A.L.G. led the analysis and the writing of the article. C.L. developed the thermal model described in the Supplementary Information and used for the analysis of the data. M.J. contributed to the data acquisition and calibration. G.C., G.T., O.B., A.L., C.S. and M.M. contributed to the geodynamical interpretation of the results. C.H. calibrated and mapped the CIRS observation of the SPT shown in Fig. 2d. R.K. conducted the radarclinometry analysis presented in the Supplementary Information. All authors contributed to the discussions and commented on the manuscript.

Additional information

Supplementary information is available for this paper.

Reprints and permissions information is available at www.nature.com/reprints.

Correspondence and requests for materials should be addressed to A.L.G.

How to cite this article: Le Gall, A. *et al.* Thermally anomalous features in the subsurface of Enceladus's south polar terrain. *Nat. Astron.* **1,** 0063 (2017).

Competing interests

The authors declare no competing financial interests.